

## H $\alpha$ EQUIVALENT WIDTHS FROM THE 3D-HST SURVEY: EVOLUTION WITH REDSHIFT AND DEPENDENCE ON STELLAR MASS

MATTIA FUMAGALLI<sup>1</sup>, SHANNON G. PATEL<sup>1</sup>, MARIJN FRANX<sup>1</sup>, GABRIEL BRAMMER<sup>2</sup>, PIETER VAN DOKKUM<sup>3</sup>, ELISABETE DA CUNHA<sup>5</sup>, MARISKA KRIEK<sup>4</sup>, BRITT LUNDGREN<sup>3</sup>, IVELINA MOMCHEVA<sup>3</sup>, HANS-WALTER RIX<sup>5</sup>, KASPER B. SCHMIDT<sup>5</sup>, ROSALIND E. SKELTON<sup>3</sup>, KATHERINE E. WHITAKER<sup>3</sup>, IVO LABBE<sup>1</sup>, ERICA NELSON<sup>3</sup>

*Accepted for publication in The Astrophysical Journal Letters*

### ABSTRACT

We investigate the evolution of the H $\alpha$  equivalent width, EW(H $\alpha$ ), with redshift and its dependence on stellar mass, using the first data from the 3D-HST survey, a large spectroscopic Treasury program with the HST-WFC3. Combining our H $\alpha$  measurements of 854 galaxies at  $0.8 < z < 1.5$  with those of ground based surveys at lower and higher redshift, we can consistently determine the evolution of the EW(H $\alpha$ ) distribution from  $z=0$  to  $z=2.2$ . We find that at all masses the characteristic EW(H $\alpha$ ) is decreasing towards the present epoch, and that at each redshift the EW(H $\alpha$ ) is lower for high-mass galaxies. We find  $EW(H\alpha) \sim (1+z)^{1.8}$  with little mass dependence. Qualitatively, this measurement is a model-independent confirmation of the evolution of star forming galaxies with redshift. A quantitative conversion of EW(H $\alpha$ ) to sSFR (specific star-formation rate) is model dependent, because of differential reddening corrections between the continuum and the Balmer lines. The observed EW(H $\alpha$ ) can be reproduced with the characteristic evolutionary history for galaxies, whose star formation rises with cosmic time to  $z \sim 2.5$  and then decreases to  $z = 0$ . This implies that EW(H $\alpha$ ) rises to 400 Å at  $z = 8$ . The sSFR evolves faster than EW(H $\alpha$ ), as the mass-to-light ratio also evolves with redshift. We find that the sSFR evolves as  $(1+z)^{3.2}$ , nearly independent of mass, consistent with previous reddening insensitive estimates. We confirm previous results that the observed slope of the sSFR- $z$  relation is steeper than the one predicted by models, but models and observations agree in finding little mass dependence.

*Subject headings:* galaxies: evolution galaxies: formation galaxies: high-redshift

### 1. INTRODUCTION

Several studies have combined different star formation indicators in order to study the evolution of star-forming galaxies (SFGs) with redshift. At a given redshift low mass galaxies typically form more stars per unit mass (i.e., specific star-formation rate, sSFR) than more massive galaxies (Juneau et al. 2005, Zheng et al. 2007, Damen et al. 2009). In addition the sSFR of galaxies with the same mass increases at higher redshift. However, semi-analytical models and observations are at odds with regards to the rate of decline of the sSFR towards low-redshift (Damen et al. 2009, Guo et al. 2010).

One of the main observational caveats is that most of the studies covering a wide redshift range use diverse SFR indicators (such as UV, IR, [OII], H $\alpha$ , SED fitting). This is a consequence of the fact that it is difficult to use the same indicator over a wide range of redshifts. One therefore has to rely on various conversion factors, often intercalibrated at  $z = 0$  and re-applied at higher redshift.

A well-calibrated standard indicator of the SFR is the H $\alpha$  luminosity (Kennicutt, 1998). However, H $\alpha$  is shifted

into the infrared at  $z > 0.5$ , and it is difficult to measure due to the limitations of ground-based near-IR spectroscopy. Comparing measures of H $\alpha$  at different redshifts has therefore been a challenge. Most of the H $\alpha$  studies at high redshift are based on narrow-band photometry (e.g. the HiZELS survey, Geach et al. 2008).

The 3D-HST survey (Brammer et al., 2012) provides a large sample of rest-frame optical spectra with the WFC3 grism, which includes the H $\alpha$  emission in the redshift range  $0.8 < z < 1.5$ . Taking advantage of the first data from the survey (45% of the final survey products) we investigate for the first time the star formation history (SFH) of the Universe with H $\alpha$  spectroscopy, using a consistent SFR indicator over a wide redshift range.

We evaluate the dependence of the H $\alpha$  Equivalent Width, EW(H $\alpha$ ), on stellar mass ( $M_*$ ) and redshift (up to  $z \sim 2$ ), comparing the 3D-HST data with other surveys in mass selected samples with  $M_* > 10^{10} M_\odot$ . Since EW(H $\alpha$ ) is defined as the ratio of the H $\alpha$  luminosity to the underlying stellar continuum, it represents a measure of the the current to past average star formation. It is therefore a model independent, directly observed proxy for sSFR.

We also derive SFRs from the H $\alpha$  fluxes. We evaluate the mean sSFR in stellar mass bins and study its evolution with redshift. The slope of the sSFR- $z$  relation in different mass bins indicates how fast the star formation is quenched in galaxies of various masses. Finally, we compare our findings to other studies (both observations and models), discussing the physical implications and reasons for any disagreements.

<sup>1</sup> Leiden Observatory, Leiden University, P.O. Box 9513, 2300 RA Leiden, Netherlands

<sup>2</sup> European Southern Observatory, Alonso de Crdova 3107, Casilla 19001, Vitacura, Santiago, Chile

<sup>3</sup> Department of Astronomy, Yale University, New Haven, CT 06511, USA

<sup>4</sup> Department of Astronomy, University of California, Berkeley, CA 94720, USA

<sup>5</sup> Max Planck Institute for Astronomy (MPIA), Knigstuhl 17, 69117 Heidelberg, Germany

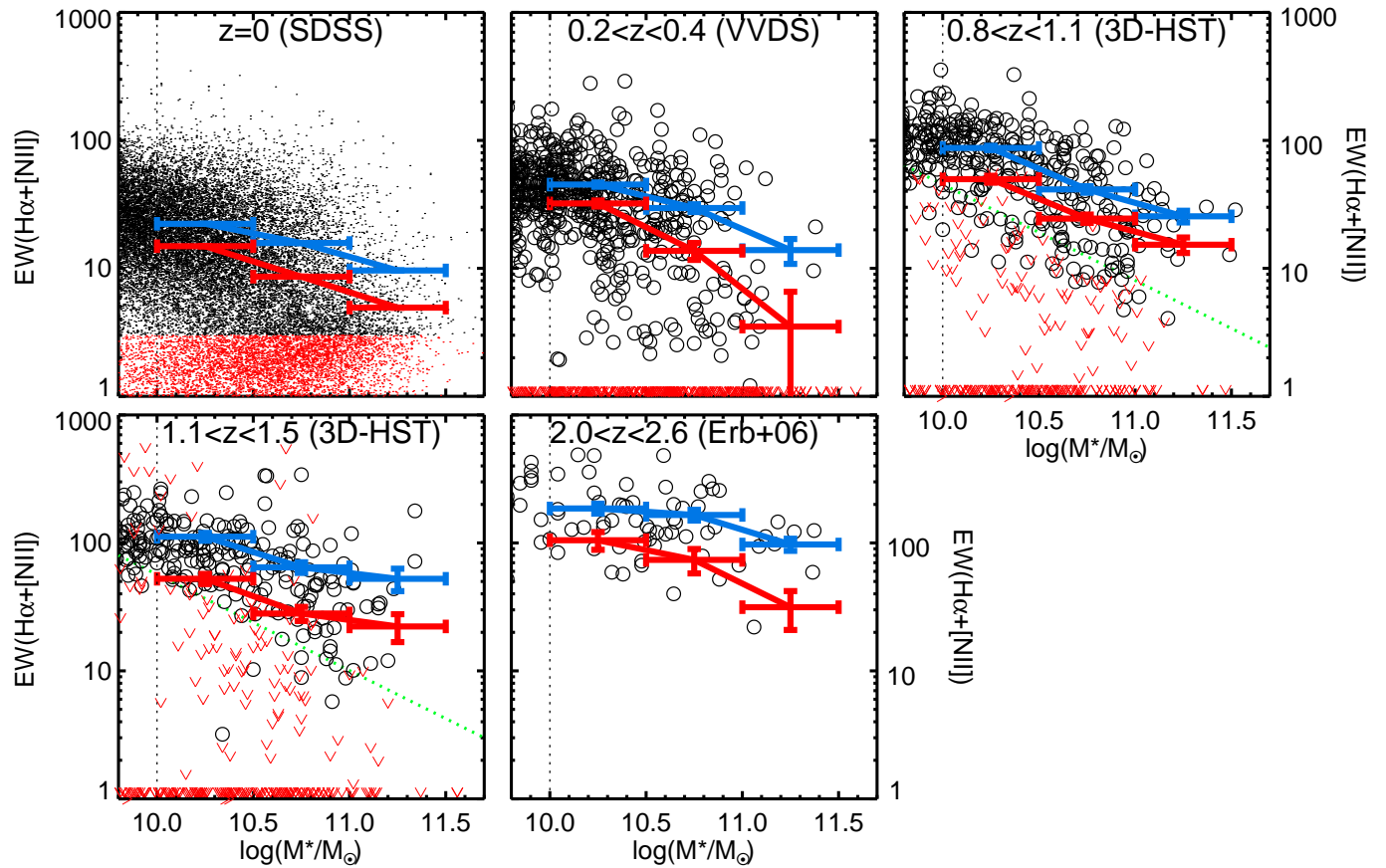


FIG. 1.—  $\text{EW}(\text{H}\alpha)$  against mass, for different redshift samples. Vertical lines represent the limiting mass of the analysis. Black symbols are objects with  $\text{H}\alpha$  detection with  $S/N > 3$  and red arrows represent upper limits. The green diagonal lines represent the detection limit of the 3D-HST data. Blue solid lines represent the mean  $\text{EW}(\text{H}\alpha)$  of detected SFGs, in 0.5 dex mass bins. Red solid lines represent the mean  $\text{EW}(\text{H}\alpha)$  of all galaxies, assuming  $\text{EW}(\text{H}\alpha)=0$  for non-detected objects. Errors of the means are computed with a bootstrap approach. At each redshift higher mass galaxies have lower  $\text{EW}(\text{H}\alpha)$  than less massive objects.

## 2. DATA

### 2.1. 3D-HST

We select the sample from the first available 3D-HST data. They include 25 pointings in the COSMOS field, 6 in GOODS-South, 12 in AEGIS, 28 in GOODS-North<sup>6</sup>. Spectra have been extracted with the aXe code (Kummel et al., 2009). Redshifts have been measured via the combined photometric and spectroscopic information using a modified version of the EAZY code (Brammer, van Dokkum, Coppi, 2008), as shown in Brammer et al. (2012). Stellar masses were determined using the FAST code by Kriek et al. (2009), using Bruzual & Charlot (2003) models and assuming a Chabrier (2003) IMF. The FAST fitting procedure relies on photometry from the NMBS catalogue (Whitaker et al. 2011) for the COSMOS and AEGIS fields, the MODS catalog for the GOODS-N (Kajisawa et al. 2009) and the FIREWORKS catalogue for GOODS-S (Wuyts et al. 2008).

The mass completeness limit is  $\log(M_*/M_\odot) > 10$  at  $z=1.5$  (Wake et al. 2011, Kajisawa et al. 2010). We select objects with  $0.8 < z < 1.5$ ; this resulted in a sample of 2121 galaxies with  $\log(M_*/M_\odot) > 10$ .

In slitless spectroscopy, spectra can be contaminated

by overlapping spectra of neighboring galaxies. The aXe package provides a quantitative estimate of the contamination as a function of wavelength, which can be subtracted from the spectra. We conservatively use spectra where the average contribution of contaminants is lower than 10% and for which more than 75% of the spectrum falls on the detector. After this selection we have 854 objects in the redshift range  $0.8 < z < 1.5$  (40% of the objects). The final sample is not biased with respect to the mass relative to the parent sample.

Line fluxes and EWs were measured as follows.<sup>7</sup> We fit the 1D spectra with a gaussian profile plus a linear continuum in the region where  $\text{H}\alpha$  is expected to lie. We subtract the continuum from the fit and measure the residual flux within  $3\sigma$  from the line center of the gaussian. Errors are evaluated including the contribution from the error on the continuum. We distinguish between detections and non-detections of  $\text{H}\alpha$  with a  $S/N$  threshold of 3. The typical  $3\sigma$  detection limit corresponds to  $\text{SFR} = 2.8 M_\odot \text{yr}^{-1}$  at  $z=1.5$  (Equation 2).

Due to the low resolution of the WFC3 grism, the  $\text{H}\alpha$  and  $[\text{NII}]$  lines are blended. In this work  $\text{EW}(\text{H}\alpha)$  therefore includes the contribution from  $[\text{NII}]$ . For the other

<sup>6</sup> From program GO-11600 (PI: B. Weiner)

<sup>7</sup> Through the entire paper the quoted EWs are rest-frame values.

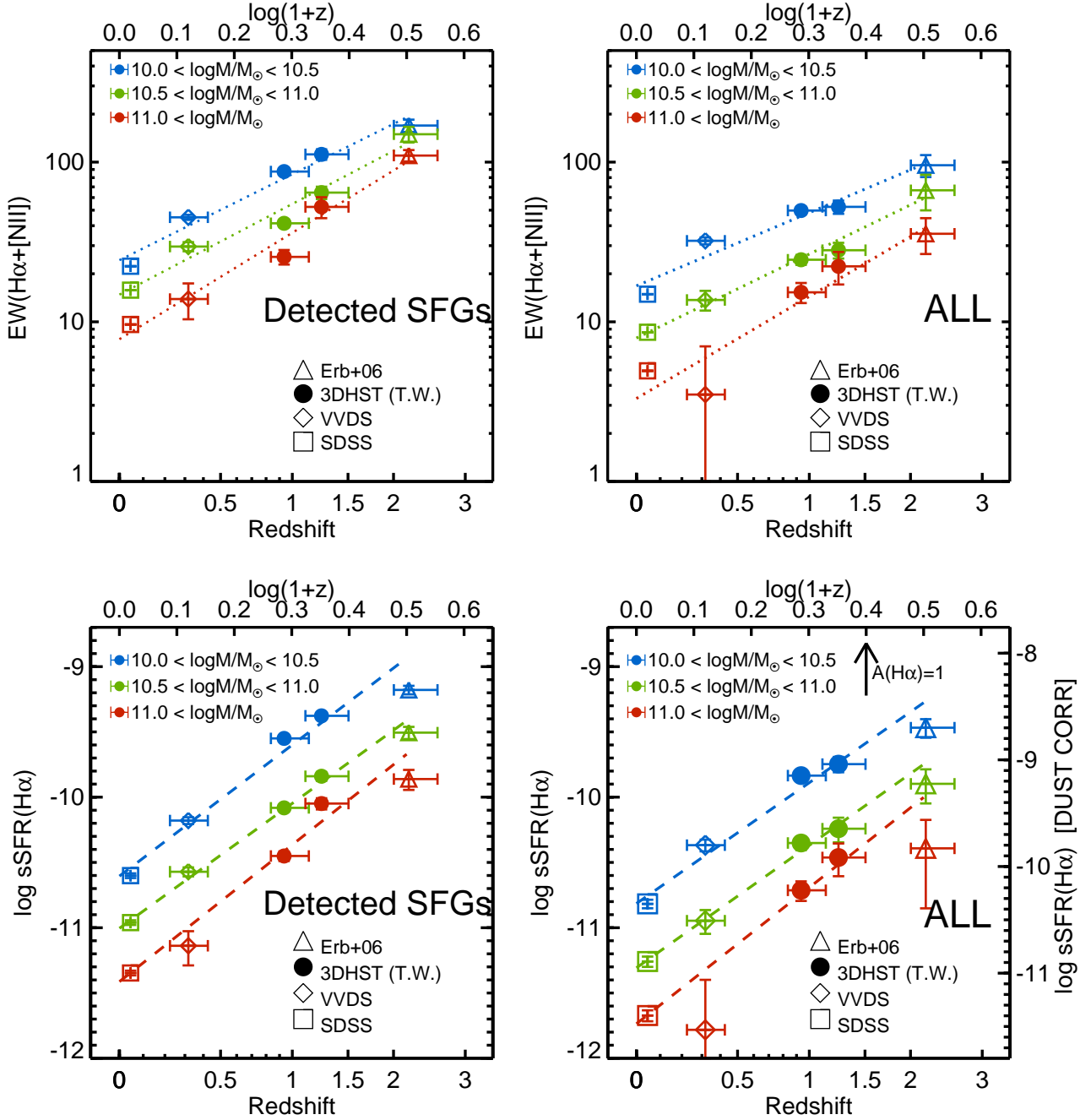


FIG. 2.— Evolution of EW(H $\alpha$ ) (top) and sSFR(H $\alpha$ ) (bottom) with redshift, in different mass bins, for SFGs (left) and all objects (right). Errors on the average EWs have been evaluated through bootstrapping. Dotted lines are the best fit power laws  $\text{EW}(z) \sim (1+z)^p$ . At fixed mass the average EW(H $\alpha$ ) and sSFR(H $\alpha$ ) increase with redshift, with a power law of  $\text{EW}(\text{H}\alpha) \sim (1+z)^{1.8}$  and  $\text{sSFR}(\text{H}\alpha) \sim (1+z)^{3.3}$  with little mass dependence. The effect of a luminosity dependent dust correction (Garn et al. 2010) correction is shown by the right axis. The effect of  $A(\text{H}\alpha)=1$  is shown by the black arrow.

datasets, which have higher spectral resolution, we combine H $\alpha$  and [NII] for consistency with 3D-HST.

## 2.2. SDSS

We retrieve masses and EW(H $\alpha$ ) for the SDSS galaxies from the MPA-JHU catalogue of the SDSS-DR7. Masses are computed based on fits to the photometry, following Kauffmann et al. (2003) and Salim et al. (2007). At redshift  $0.03 < z < 0.06$ , for masses higher than  $M_* = 10^{10} M_{\odot}$ , the SDSS sample is spectroscopically

complete in stellar mass (Jarle Brinchmann, private communication). We consider as detections only measurements greater than  $3\text{\AA}$ , as the ones with  $\text{EW} < 3\text{\AA}$  are affected by uncertainties in the stellar continuum subtraction (Jarle Brinchmann, private communication).

In the redshift range  $0.03 < z < 0.06$ , the spectroscopic fiber of SDSS does not cover the entirety of most galaxies. As a consequence sSFR are evaluated with emission line fluxes and masses from the fiber alone.

### 2.3. VVDS

The VIMOS VLT Deep Survey (VVDS, Le Fevre et al. 2005) is a wide optical selected survey of distant galaxies.  $H\alpha$  is covered by the VIMOS spectrograph at  $0.0 < z < 0.4$ .

Lamareille et al. (2009) released a catalog of 20,000 galaxies with line measurements, complete down to  $M_* = 10^{9.5}M_\odot$  at  $z = 0.5$ . Masses are retrieved from the VVDS catalog; they have been computed through a Bayesian approach based on photometry (equivalent to Kauffmann et al. 2003 and Tremonti et al. 2004), and are relative to a Chabrier IMF. We select a sample with redshift  $0.2 < z < 0.4$  and  $M_* > 10^{10.0}M_\odot$  containing 741 objects, of which 477 (64 %) have an  $H\alpha$  measurement with  $S/N > 3$ . The percentage of  $H\alpha$  detected objects drops to 32% at masses  $M_* > 10^{11.0}M_\odot$ .

### 2.4. High redshift data

Erb et al. (2006) published  $EW(H\alpha)$  for galaxies selected with the BX criterion (Steidel et al. 2004), targeting SFGs at redshift  $2.0 < z < 2.5$ . We evaluate the completeness of the sample as follows. From the FIREWORKS catalogue (Wuyts et al. 2008) we reconstruct the BX selection and evaluate the fraction of objects with spectroscopically confirmed redshift  $2.0 < z < 2.5$  that fall in the BX selection. Percentages are 44%, 32% and 27% for mass limited samples with  $\log(M_*/M_\odot) = 10.0-10.5$ ,  $\log(M_*/M_\odot) = 10.5-11$ ,  $\log(M_*/M_\odot) > 11.0$ .

## 3. THE $EW(H\alpha)$ - MASS RELATION

We first study how  $EW(H\alpha)$  depends on stellar mass in each available data set. The 3D-HST sample has been divided in two redshift bins,  $0.8 < z < 1.1$  and  $1.1 < z < 1.5$ . The results are shown in Figure 1. At each redshift, highest mass galaxies have lower  $EW(H\alpha)$ . Note however, that there is a large scatter in the relation. We quantify the trend in the following way: we determine the average  $EW(H\alpha)$  in three 0.5 dex wide mass bins ( $10.0 < \log(M_*/M_\odot) < 10.5$ ,  $10.5 < \log(M_*/M_\odot) < 11$ ,  $\log(M_*/M_\odot) > 11.0$ ) and evaluated its error through bootstrapping the sample. The mean  $EW(H\alpha)$  in a given mass bin is obtained in two ways: (1) using only detected, highly SFGs (blue lines in Figure 1) and (2) using all galaxies but assigning  $EW(H\alpha)=0$  to the objects detected in  $H\alpha$  with  $S/N < 3$  (red lines in Figure 1). For the  $z = 2.2$  data, we use the the FIREWORKS catalog to establish the fraction of galaxies excluded by the BX selection and therefore give an estimation of  $EW(H\alpha)$  for all galaxies.

Using either method we find that an  $EW(H\alpha)$ -mass relation is in place at each redshift, not just for strongly star forming objects but also for the entire galaxy population. Galaxies in the lowest mass bin ( $10.0 < \log(M_*/M_\odot) < 10.5$ ) have on average an  $EW(H\alpha)$  which is 5 times higher than galaxies in the highest mass bin ( $\log(M_*/M_\odot) > 11.0$ ).

We discuss the evolution of the  $EW(H\alpha)$ -mass relation with redshift in the next section of the Letter. However, it is immediately evident from Figure 1 that the 3D-HST survey targets galaxies with  $EW(H\alpha)$  typical of an intermediate regime between what is seen at  $z=0$  and what is seen at higher redshift. In other words the  $EW(H\alpha)$ -mass relation seems to rigidly shift towards higher  $EW(H\alpha)$  at

higher redshifts.

A considerable fraction of detected galaxies in 3D-HST have  $EW(H\alpha) > 30\text{\AA}$ , while in SDSS similar objects are extremely rare: 3.8%, 1.4% and 0.4% for increasing mass samples. This study can be seen as an extension of the findings of van Dokkum et al. (2011), who reported that massive galaxies at  $z > 1$  show a wider range of  $EW(H\alpha)$  compared to galaxies in the local Universe. Following this trend with redshift, in the  $z > 2$  bin we find typical  $EW(H\alpha)$  of 150  $\text{\AA}$  for SFGs. Such high values of  $EW(H\alpha)$  represent just 11% of the 3D-HST sample (14.6%, 8.1% and 4.7% respectively for increasing mass bins).

## 4. THE EVOLUTION OF $EW(H\alpha)$ WITH REDSHIFT

The evolution of  $EW(H\alpha)$  with redshift can be seen as an observational (i.e. model-independent) proxy for the  $sSFR-z$  relation. Figure 2 (top panels) shows the redshift evolution of the average  $EW(H\alpha)$  in different mass bins for the detected SFGs (top left panel) and for all galaxies (top right panel). A substantial increase of the  $EW(H\alpha)$  is seen at higher redshifts in both samples. We therefore infer that evolution of the SFR is not a byproduct of selection effects from different SFR indicators. At  $0.8 < z < 1.5$ , a galaxy has on average an  $EW(H\alpha)$  that is 3-4 times higher than that of an object of comparable mass in the local universe. For each mass bin we parametrize the redshift evolution of the  $EW(H\alpha)$  as follows:

$$EW(H\alpha)(z) \sim A \times (1+z)^p \quad (1)$$

The coefficient  $p$  has an average value of 1.8, with little dependence on mass (best fit values are listed in Table 1). As can be deduced from Table 1 there may be a weak mass dependence such that the relations steepen with mass; however, the difference between the slopes at the lowest and highest mass bin is not statistically significant.

This indicates that the decrease of  $EW(H\alpha)$  happens at the same rate for all galaxies irrespectively of their masses. As seen in the right panel of Figure 2, the addition of non-SFGs amounts to a negative vertical shift in the  $EW(H\alpha)$  but not to a change in the slope of the relation.

An uncertainty is the effect of dust on the  $EW(H\alpha)$ . Without more measurements we cannot state what effect dust has, and in literature there is disagreement on the relative extinction suffered by the nebular emission lines and the underlying stellar continuum (Calzetti et al. 2000, Erb et al. 2006, Wuyts et al. 2011). However, the data motivated model described in Section 6 suggests that dust has a mild effect on the  $EW(H\alpha)$ .

## 5. THE $sSFR(H\alpha)$ - MASS RELATION AND ITS EVOLUTION WITH REDSHIFT

The  $EW(H\alpha)$  has the advantage that it is a direct observable, but it is more difficult to interpret than a more physical quantity like the specific star formation rate. The latter can only be derived with a proper extinction correction for  $H\alpha$ . We lack this information, as we do not have a proper Balmer decrement measurement. In the following we briefly explore the specific star formation rate ( $sSFR$ ) evolution implied by assuming no extinction and later discuss the effect of a dust correction to the measured slopes of the  $sSFR-z$  relation.

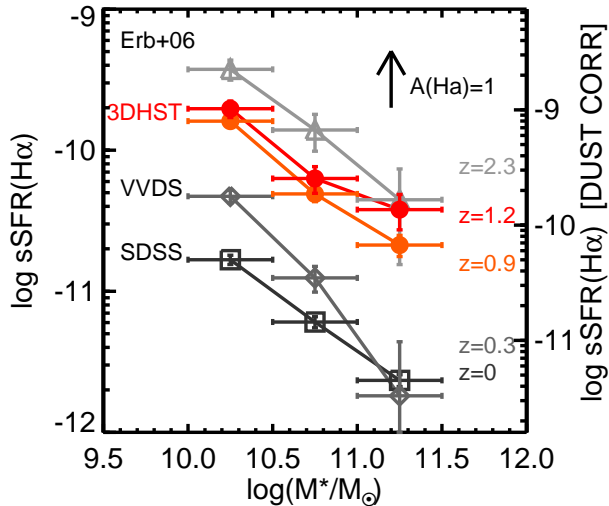


FIG. 3.— Mean values of sSFR(H $\alpha$ ) in 0.5 dex mass bins at various redshift for SDSS, VVDS, 3D-HST and from Erb et al. (2006). At each redshift more massive galaxies have less sSFR(H $\alpha$ ) than less massive ones. The effect of a luminosity dependent dust correction (Garn et al. 2010) correction is shown by the right axis. The effect of  $A(\text{H}\alpha)=1$  is shown by the black arrow.

The SFR is derived from the H $\alpha$  flux<sup>8</sup> using Kennicutt (1998):

$$\text{SFR}(\text{H}\alpha)[M_{\odot}\text{yr}^{-1}] = 7.9 \times 10^{-42} \times L(\text{H}\alpha)[\text{erg/s}] \times 10^{-0.24} \quad (2)$$

where the  $10^{-0.24}$  factor accounts for a conversion to the Chabrier IMF, from Salpeter (as in Muzzin et al. 2010).

Figure 3 shows the mean value of sSFR(H $\alpha$ ) in different stellar mass bins, at different redshifts. In each redshift bin higher mass galaxies have lower sSFR(H $\alpha$ ).

In Figure 2 (bottom panels) we show the redshift evolution of the average sSFR(H $\alpha$ ) in different mass bins for detected SFGs (bottom left panel) and for all galaxies (bottom right panel). A typical galaxy at  $z=1.5$  has as sSFR(H $\alpha$ ) 15-20 times higher than a galaxy of the same mass at  $z=0$ . In each mass bin we fit the evolution of the sSFR in redshift with a power law:

$$\text{sSFR}(z) \sim B_M \times (1+z)^n \quad (3)$$

obtaining a value of  $n = 3.2 \pm 0.1$ . As can be deduced from Table 1 there may be a weak mass dependence such that the relations steepen with mass; however, the slopes at the lowest and highest mass bin are not statistically different.

The sSFR- $z$  relation is steeper than the EW- $z$  relation, because of the additional evolution of the M/L ratio:

$$\text{EW}/\text{sSFR} \sim L(\text{H}\alpha)/L_R \times M_*/(K * L(\text{H}\alpha)) \sim M/L_R \quad (4)$$

where  $K$  is the conversion factor in Equation 2 and  $L_R$  is the R-band luminosity.

Implementing a luminosity dependent dust correction for H $\alpha$  (Garn et al. 2010, shown with the right axis in Figure 2, bottom right) would increase the value of  $n$  to  $3.7 \pm 0.1$ . However, several studies (Sobral et al. 2012,

<sup>8</sup> We assume a  $[\text{NII}]/(\text{H}\alpha + [\text{NII}])$  ratio of 0.25 for the 3D-HST sources.

Dominguez et al. 2012, Momcheva et al., submitted) have indicated that a better indicator for the H $\alpha$  extinction at different redshifts is the stellar mass, and that the H $\alpha$  extinction depends strongly on mass but little on redshift (at constant mass). The Garn & Best 2010 relation gives median  $A(\text{H}\alpha)$  of 1, 1.5 and 1.7 mag for the increasing mass bins in this study. A mass-dependent dust correction impacts the normalization of the sSFR but not the slope  $n$ .

Our implied evolution of the sSFR compares well to results from literature. For example, Damen et al. (2009) found  $n = 4 \pm 1$  based on UV + IR inferred sSFRs, and Karim et al. (2011) found  $n = 3.50 \pm 0.02$  for SFGs and  $n = 4.29 \pm 0.03$  for all galaxies, based on stacked radio imaging.

All results indicate an evolution which is steeper with redshift than semianalytical models (Guo & White 2008, Guo et al. 2011), who find slopes close to  $n=2.5$ . All studies find that the slope does not depend on the stellar mass out so  $z=2$ . In short, our results are consistent with previous determinations.

## 6. LINKING THE CHARACTERISTIC SFH OF GALAXIES AND EW(H $\alpha$ )

We compare the observed evolution of EW(H $\alpha$ ) to what might be expected from other observations. We construct the typical SFH of a galaxy with mass  $\sim 10^{11}M_{\odot}$  at  $z=0$ . As a starting point, we assume that the cumulative number density remains constant with redshift (similar to van Dokkum et al. 2010, Papovich et al. 2011, Patel et al. 2012). We use the mass functions of Marchesini et al. (2009) and Papovich et al. (2011), and we show the resulting mass evolution in Figure 4c. We determine the SFR at these masses from Damen et al. (2009), Papovich et al. (2011) and Smit et al. (2012), and we fit a simple curve to these values (indicated by the curve in Figure 4a). This evolutionary history reproduces the mass evolution well (Figure 4c).

Next we calculate the implied EW(H $\alpha$ ):  $L(\text{H}\alpha)$  is derived using Equation 2, and Bruzual & Charlot 2003 models are used to calculate the stellar continuum, assuming solar metallicity (Figure 4b). The predicted EW(H $\alpha$ ) rises monotonically to high redshift, reaching 400Å at  $z=8$  (Figure 4d). The predicted EW(H $\alpha$ ) corresponds surprisingly well to the observed EW(H $\alpha$ ) Even the  $z=4$  detections by Shim et al. (2011) based on broadband IRAC photometry are consistent within the errors. Apparently, our simple method produces a robust prediction of the evolution of EW(H $\alpha$ ). We note that the implied sSFR (Figure 4e) is higher than expected from straight measurement of  $L(\text{H}\alpha)$ , consistently with significant dust extinction. One magnitude of extinction for H $\alpha$  is needed to reconcile this discrepancy.

It is remarkable that our prediction worked well for EW(H $\alpha$ ): the average evolution of galaxies was derived from the evolution of the mass function and SFR, which carry significant (systematic) uncertainties when derived from observations; whereas the EW(H $\alpha$ ) is a direct observable.

## 7. CONCLUSIONS

We have used the 3D-HST survey to measure the evolution of the EW(H $\alpha$ ) from  $z=0$  to  $z=2$ . We show that the EW(H $\alpha$ ) evolves strongly with redshift, at a con-

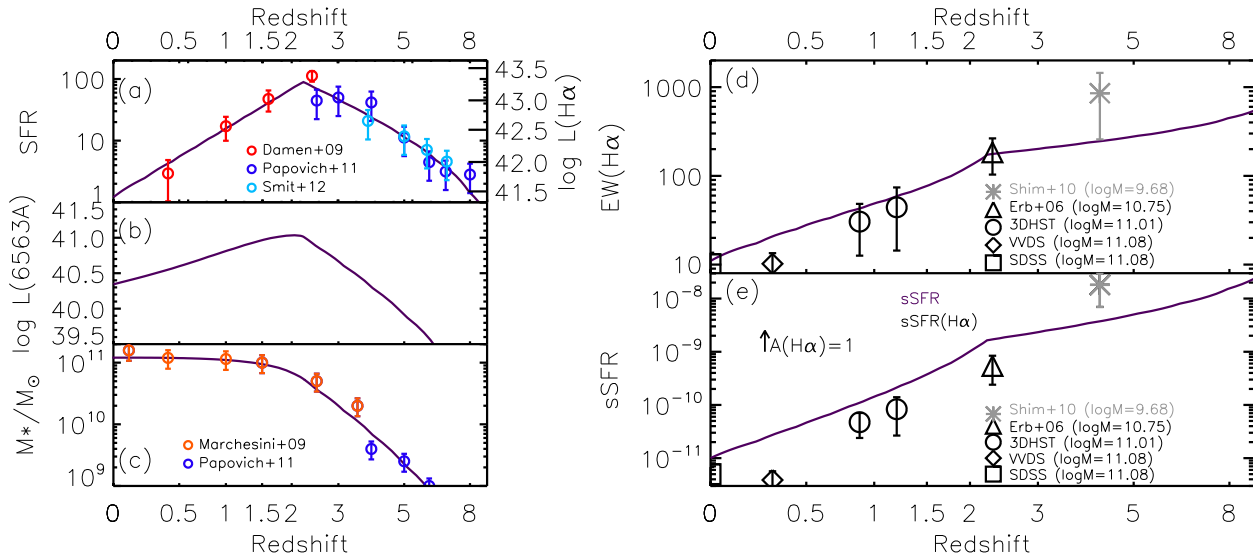


FIG. 4.— Comparison of observed  $EW(H\alpha)$  with predictions from a simple observational supported model, at different redshifts. (a) Input SFH, and  $H\alpha$  Luminosity (b) Luminosities at  $6563 \text{ \AA}$ , from the Bruzual & Charlot 2003 code. (c) Mass growth. (d) Evolution of  $EW(H\alpha)$  with redshift. (e) Evolution of  $sSFR$  with redshift. Data points are mean  $EW(H\alpha)/sSFR(H\alpha)$  of observed galaxies with mass in a 0.3 dex bin around the typical mass of the model at a given redshift.

stant mass, like  $(1+z)^{1.8}$ . The evolution is independent of stellar mass. The equivalent width goes down with mass (at constant redshift). The increase with redshift demonstrates the strong evolution of star forming galaxies, using a consistent and completely model independent indicator. We explore briefly the implied  $sSFR$  evolution, ignoring dust extinction. We find that the evolution with redshift is strong ( $sSFR \sim (1+z)^{3.2}$ ). This stronger evolution is expected as the mass-to-light ratio of galaxies evolves with time, and this enters the correction from  $EW$  to  $sSFR$ . The increase with redshift is faster than predicted by semi-analytical models (e.g., Guo & White 2008), consistent with earlier results.

We construct the characteristic SFH of a  $10^{11}M_{\odot}$  galaxy. This simple history reproduces the observed evolution of the  $EW(H\alpha)$  to  $z=2.5$ , and even to  $z=4$ . It implies that the  $EW(H\alpha)$  continue to increase to higher redshifts, up to  $400 \text{ \AA}$  at  $z=8$ . This has a significant im-

pact for the photometry and spectroscopy of these high redshift sources.

The study can be expanded in the future when the entire 3D-HST survey will be available, doubling the sample and including the ACS grism. In addition to increased statistics, the ACS grism will allow evaluation of the Balmer decrement and therefore a precise dust corrected evaluation of SFR. Moreover, a statistically significant  $H\alpha$  sample at  $z \sim 1$  will be central to understand the composition, the scatter and the physical origin of the so called 'star-forming-main sequence'.

We thank the referee for providing valuable comments, and Jarle Brinchmann, David Sobral and Simone Weinmann for useful discussions. We acknowledge funding from ERC grant HIGHZ no. 227749.

#### REFERENCES

- Brammer, G. B., van Dokkum, P. G., & Coppi, P. 2008, *ApJ*, 686, 1503
- Brammer, G., van Dokkum, P., Franx, M., et al. 2012, [arXiv:1204.2829](https://arxiv.org/abs/1204.2829)
- Bruzual, G., & Charlot, S. 2003, *MNRAS*, 344, 1000
- Calzetti, D., Armus, L., Bohlin, R. C., et al. 2000, *ApJ*, 533, 682
- Chabrier, G. 2003, *ApJ*, 586, L133
- Damen, M., Förster Schreiber, N. M., Franx, M., et al. 2009, *ApJ*, 705, 617
- Damen, M., Labbé, I., van Dokkum, P. G., et al. 2011, *ApJ*, 727, 1
- Domínguez, A., Siana, B., Henry, A. L., et al. 2012, [arXiv:1206.1867](https://arxiv.org/abs/1206.1867)
- Erb, D. K., Steidel, C. C., Shapley, A. E., et al. 2006, *ApJ*, 647, 128
- Garn, T., & Best, P. N. 2010, *MNRAS*, 409, 421
- Garn, T., Sobral, D., Best, P. N., et al. 2010, *MNRAS*, 402, 2017
- Geach, J. E., Smail, I., Best, P. N., et al. 2008, *MNRAS*, 388, 1473
- Guo, Q., & White, S. D. M. 2008, *MNRAS*, 384, 2
- Guo, Q., White, S., Li, C., & Boylan-Kolchin, M. 2010, *MNRAS*, 404, 1111
- Guo, Q., White, S., Boylan-Kolchin, M., et al. 2011, *MNRAS*, 413, 101
- Juneau, S., Glazebrook, K., Crampton, D., et al. 2005, *ApJ*, 619, L135
- Kajisawa, M., Ichikawa, T., Tanaka, I., et al. 2009, *ApJ*, 702, 1393
- Kajisawa, M., Ichikawa, T., Yamada, T., et al. 2010, *ApJ*, 723, 129
- Karim, A., Schinnerer, E., Martínez-Sansigre, A., et al. 2011, *ApJ*, 730, 61
- Kauffmann, G., Heckman, T. M., White, S. D. M., et al. 2003, *MNRAS*, 341, 33
- Kennicutt, R. C., Jr. 1998, *ApJ*, 498, 541
- Kriek, M., van Dokkum, P. G., Labbé, I., et al. 2009, *ApJ*, 700, 221
- Kümmel, M., Walsh, J. R., Pirzkal, N., Kuntschner, H., & Pasquali, A. 2009, *PASP*, 121, 59
- Lamareille, F., Brinchmann, J., Contini, T., et al. 2009, *A&A*, 495, 53
- Le Fèvre, O., Vettolani, G., Garilli, B., et al. 2005, *A&A*, 439, 845
- Marchesini, D., van Dokkum, P. G., Förster Schreiber, N. M., et al. 2009, *ApJ*, 701, 1765

- Momcheva, I., Lee, J. C., Ly, C., et al. 2012, arXiv:1207.5479  
Muzzin, A., van Dokkum, P., Kriek, M., et al. 2010, ApJ, 725, 742  
Papovich, C., Finkelstein, S. L., Ferguson, H. C., Lotz, J. M., & Giavalisco, M. 2011, MNRAS, 412, 1123  
Patel, S. G., van Dokkum, P. G., Franx, M., et al. 2012, arXiv:1208.0341  
Salim, S., Rich, R. M., Charlot, S., et al. 2007, ApJS, 173, 267  
Shim, H., Chary, R.-R., Dickinson, M., et al. 2011, ApJ, 738, 69  
Smit, R., Bouwens, R. J., Franx, M., et al. 2012, arXiv:1204.3626  
Sobral, D., Best, P. N., Matsuda, Y., et al. 2012, MNRAS, 420, 1926  
Steidel, C. C., Shapley, A. E., Pettini, M., et al. 2004, ApJ, 604, 534  
Tremonti, C. A., Heckman, T. M., Kauffmann, G., et al. 2004, ApJ, 613, 898  
van Dokkum, P. G., Whitaker, K. E., Brammer, G., et al. 2010, ApJ, 709, 1018  
van Dokkum, P. G., Brammer, G., Fumagalli, M., et al. 2011, ApJ, 743, L15  
Wake, D. A., Whitaker, K. E., Labbé, I., et al. 2011, ApJ, 728, 46  
Whitaker, K. E., Labbé, I., van Dokkum, P. G., et al. 2011, ApJ, 735, 86  
Wuyts, S., Labbé, I., Schreiber, N. M. F., et al. 2008, ApJ, 682, 985  
Wuyts, S., Förster Schreiber, N. M., Lutz, D., et al. 2011, ApJ, 738, 106  
Zheng, X. Z., Bell, E. F., Papovich, C., et al. 2007, ApJ, 661, L41

TABLE 1  
SLOPES OF EW- $z$  AND sSFR- $z$  RELATION

$\log(M_*/M_\odot)$	EW(det)	EW(all)	sSFR(det)	sSFR(all)
10.0-10.5	$1.79 \pm 0.18$	$1.52 \pm 0.21$	$3.32 \pm 0.08$	$3.06 \pm 0.13$
10.5-11.0	$1.89 \pm 0.20$	$1.75 \pm 0.13$	$3.18 \pm 0.09$	$3.11 \pm 0.18$
11.0-11.5	$2.21 \pm 0.22$	$2.12 \pm 0.43$	$3.50 \pm 0.12$	$3.45 \pm 0.26$